Improving 3D-Turbo Code's BER Performance with a BICM System over Rayleigh Fading Channel

Rugui YAO [1], *Yongjia ZHU* [1], *Juan XU* [2], *Fangqi GAO* [1], *Ling WANG* [1]

[1] School of Electronics and Information, Northwestern Polytechnical University, 710072 Xi'an, Shaanxi, China
[2] School of Electronic and Control Engineering, Chang'an University, 710064 Xi'an, Shaanxi, China

yaorg@nwpu.edu.cn, 775052163@qq.com, xuj@mail.nwpu.edu.cn, 872145959@qq.com, lingwang@nwpu.edu.cn

Manuscript received October 12, 2015

Abstract. *Classical Turbo code suffers from high error floor due to its small Minimum Hamming Distance (MHD). Newly-proposed 3D-Turbo code can effectively increase the MHD and achieve a lower error floor by adding a rate-1 post encoder. In 3D-Turbo codes, part of the parity bits from the classical Turbo encoder are further encoded through the post encoder. In this paper, a novel Bit-Interleaved Coded Modulation (BICM) system is proposed by combining rotated mapping Quadrature Amplitude Modulation (QAM) and 3D-Turbo code to improve the Bit Error Rate (BER) performance of 3D-Turbo code over Raleigh fading channel. A key-bit protection scheme and a Two-Dimension (2D) iterative soft demodulating-decoding algorithm are developed for the proposed BICM system. Simulation results show that the proposed system can obtain about 0.8-1.0 dB gain at BER of* 10^{-6}*, compared with the existing BICM system with Gray mapping QAM.*

Keywords

3D-Turbo code, rotated mapping, Bit-Interleaved Coded Modulation (BICM), key-bit protection, 2D iterative soft demodulating-decoding algorithm

1. Introduction

In 1993, Claude Berrou invented Turbo code, which is one of Shannon-limit approaching channel codes [1]. Due to its excellent convergence performance in the waterfall region, it has been adopted in many communication standards, such as *Consultative Committee for Space Data Systems* (CCSDS), *Third Generation Partnership Project* (3GPP) communication system, *Digital Video Broadcasting* (DVB), IEEE 802.16, etc. Unfortunately, Turbo code suffers from high error floor for its small MHD. Newly-proposed 3D-Turbo code effectively increases the MHD and achieves a lower error floor by adding a rate-1 post encoder. In 3D-Turbo codes, part of parity bits from the classical Turbo encoder are further encoded through the post encoder. In this paper, we consider the improvement of BER performance of 3D-Turbo code over Rayleigh fading channels.

In [2], periodic time-varying convolutional code is selected to construct post-encoder to improve the extrinsic information from pre-decoder to the two *soft-input-soft-output* (SISO) decoder. By this means, the convergence threshold of 3D-Turbo code is lowered. A novel joint coded modulation scheme combining 3D-Turbo code and high-order QAM is proposed to decrease the loss of convergence in [3]. In that scheme, the technique of unequal-error protection is utilized, where the bits with high protection capability in Gray mapping are used to transmit the key bits of 3D-Turbo codes, such as the systematic bits and the post-encoded parity bits.

In [4] and [5], a rotated mapping scheme is proposed, whose constellation can be obtained by rotating the Gray-mapping constellation with a given angle. By the rotation, the signal diversity is achieved [6]; as a result, the performance over Rayleigh fading channel is effectively improved [7]. In this paper, a BICM architecture is constructed by combining 3D-Turbo code and rotated mapping QAM. And then, a key-bit protection scheme and a 2D soft iterative demodulating-decoding algorithm are proposed for the BICM architecture. The proposed techniques are proved to improve the BER performance of 3D-Turbo code over Rayleigh fading channel.

In [8], a novel and theoretical framework for the two-dimensional iterative detection is proposed, which fully utilizes the correlation between neighboured pixels to improve the BER performance. Dr. Keith proposed an adaptive soft-input soft-Output algorithm for iterative detection with parametric uncertainty [9]. Then the algorithm was applied to joint equalization-decoding for trellis-based codes over frequency-selective channels. In our paper, we will consider the two-dimensional iterative processing combining 3D-Turbo codes and rotated mapping QAM. Our consideration is not involved in the above literatures.

The rest of this paper is organized as follows. Sections 2 and 3 briefly review the 3D-Turbo codes and the rotated mapping. Section 4 develops the key-bit protection scheme for rotated mapping. The soft demodulation of QAM is discussed with the a prior information from 3D-Turbo decoder in Sec. 5. In Sec. 6, a novel BICM system combining

3D-Turbo code and rotated mapping QAM is proposed to improve the BER performance over Rayleigh fading channel. Simulation results and conclusions are provided in Sec. 7 and 8, respectively.

2. 3D Turbo Codes

A 3D turbo encoder in [10] is depicted in Fig. 1. Compared with the classical Turbo encoder, a fraction λ of the parity bits from the constituent encoders, RSC1 and RSC2, are grouped by a *Parallel-to-Serial* (P/S) multiplexer, permuted by a permutation π', and encoded by a rate-1 convolutional post encoder whose output is denoted by **W**. The newly-added post encoder can help to decorrelate the extrinsic information from the constituent decoders of the classical Turbo decoder, which lowers down the error floor. In original references, λ is defined as the permeability rate and very simple regular permeability patterns are usually applied.

As shown in Fig. 2, the 3D Turbo decoder is comprised of a classical Turbo decoder and a pre-decoder corresponding to the post-encoder; the extrinsic information is exchanged among them. The classical iterative Turbo decoding principle is still feasible for 3D Turbo decoder. First, the pre-decoder is activated to feed the classical Turbo decoder with extrinsic information about the post-encoded parity bits. The two SISO decoders of classical Turbo decoder exchange extrinsic information about the systematic bits. They also provide the pre-decoder with extrinsic information about the post-encoded parity bits. The decoding process continues iteratively until all constituent decoders have converged, or a maximum number of iterations has been performed.

In [11], we have derived the information calculations and addressed the information exchange procedure in detail.

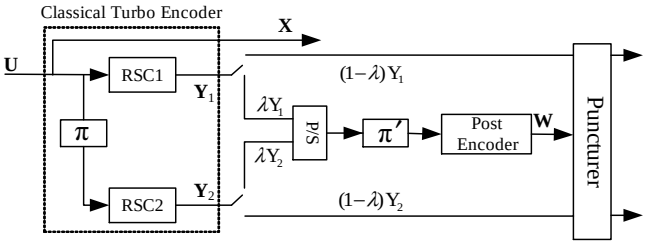

Fig. 1. 3D Turbo encoder.

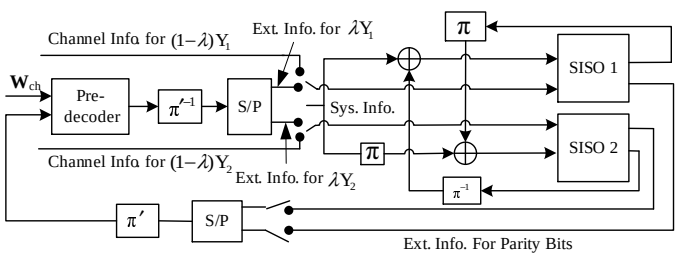

Fig. 2. 3D Turbo decoder.

3. Rotated Mapping

Rotated mapping is a kind of modulation diversity techniques implemented by rotating the constellation of classical mapping QAM [4], [6]. By the rotation, the number of different amplitudes on I and Q axes is increased, and then the modulation diversity degrees are maximized.

3.1 Classical Gray Mapping QAM

In this part, we take 16-QAM as an example to review the classical Gray mapping QAM as shown in Fig. 3. A point of 16-QAM can be mapped by a 4-bit sequence, $(b_0b_1b_2b_3)$, where b_0b_2 and b_1b_3 correspond to the coordinates on I and Q axis, respectively. 10, 11, 01 and 00 of bit pair b_0b_2 are mapped into the real coordinate of the point with value -3, -1, $+1$ and $+3$, respectively. Bit pair b_1b_3 has the same mapping relationship to construct the imaginary coordinate of the point. To normalized the transmitted power, the coordinates need multiplying a factor according to modulation order [12]. Finally, the normalized coordinates are modulated and added up to form transmitted QAM symbols.

3.2 Implementation of Rotated Mapping

The constellation of rotated mapping QAM can be constructed by rotating the classical constellation of Gray mapping QAM with a certain angle. Figure 4 shows the constellation of rotated mapping 16-QAM originating from classical constellation of Gray mapping 16-QAM, where α is the optimized rotation angle as analyzed in next subsection.

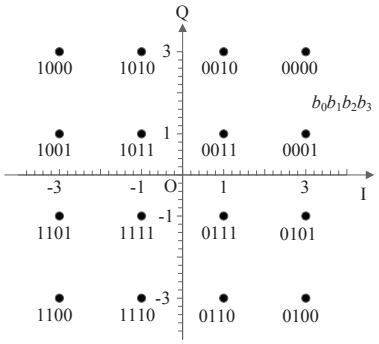

Fig. 3. Constellation of Gray mapping 16-QAM (without normalization).

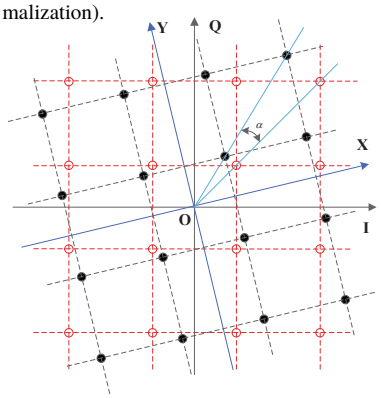

Fig. 4. Constellation of rotated mapping 16-QAM originating from constellation of Gray mapping 16-QAM.

Let $\mathbf{G} = (u_0, \cdots, u_{N-1})$ be N symbols of Gray mapping QAM, where $u_n = u_n^{\mathrm{I}} + ju_n^{\mathrm{Q}}$, $u_n^{\mathrm{I}} = \mathrm{Re}(u_n)$ and $u_n^{\mathrm{Q}} = \mathrm{Im}(u_n)$, for $n = 0, \cdots, N-1$. Further let α be the rotation angle, and thus the rotation matrix, $\mathbf{R}$, can be constructed as

$$\mathbf{R} = \begin{pmatrix} \cos\alpha & \sin\alpha \\ -\sin\alpha & \cos\alpha \end{pmatrix}. \tag{1}$$

Let $\mathbf{P} = (p_0, \cdots, p_{N-1})$ be the symbols of rotated mapping QAM corresponding to $\mathbf{G}$. The n-th symbol, $p_n = p_n^{\mathrm{I}} + jp_n^{\mathrm{Q}}$, where $p_n^{\mathrm{I}} = \mathrm{Re}(p_n)$ and $p_n^{\mathrm{Q}} = \mathrm{Im}(p_n)$ are calculated as

$$\begin{pmatrix} p_n^{\mathrm{I}} \\ p_n^{\mathrm{Q}} \end{pmatrix} = \mathbf{R} \times \begin{pmatrix} u_n^{\mathrm{I}} \\ u_n^{\mathrm{Q}} \end{pmatrix}. \tag{2}$$

For rotated mapping, we always expect the symbols on I and Q axes experience independent fading to minimize the *symbol error rate* (SER) over fading channel. Generally, a combination of the symbols on I axis and the interleaved symbols on Q axis can achieve independent fading for these two symbols. For this purpose, cyclic shift of the symbols on Q axis, p_n^{Q}, is usually and easily implemented. Assuming K-symbol cyclic shift of the symbols on Q axis, we can construct the complex transmitted symbols, $\mathbf{X} = (x_0, x_1, \cdots, x_{N-1})$, from $\mathbf{P}$, as

$$x_n = \begin{cases} p_n^{\mathrm{I}} + jp_{N-K+n}^{\mathrm{Q}} & \text{for } n = 0, \cdots, K-1 \\ p_n^{\mathrm{I}} + jp_{n-K}^{\mathrm{Q}} & \text{for } n = K, \cdots, N-1 \end{cases}. \tag{3}$$

3.3 Optimization of Rotation Angle

The demodulation performance for rotated mapping depends on the rotation angle. In [6], the rotation angle is optimized for DVB-T2 standard [12] in terms of maximizing the minimum L-product distance. The optimized rotation angles for QPSK and 16-QAM are 29.0° and 16.8°, respectively [6], [12]. Although these angles are optimized to a specific fading channel, rotated mapping QAM with them over other fading channels still outperforms classical Gray mapping QAM, as shown in [5]. Therefore, in the later discussion, we use the optimized angles for different modulations listed in [6], [12].

4. Key-Bit Protection

4.1 Unequal Error Protection of Rotated Mapping QAM

For Gray mapping QAM, different bits have different error performance, which is also called *unequal error protection* (UEP) [14]. In the following part, we will validate the rotated mapping QAM also has the UEP capability.

While the constellation of rotated mapping QAM is generated by rotating the constellation of Gray mapping QAM with an angle, decision thresholds for rotated mapping QAM can be obtained by rotating the decision thresholds for Gray mapping QAM with the same angle. Therefore, UEP can be adopted for rotated mapping QAM. First of all, we address the statistics of the noise under the rotated mapping coordinate system.

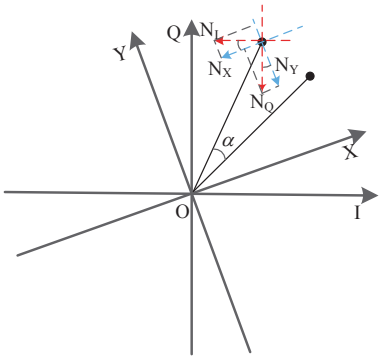

Fig. 5. The transformation of received noise between IOQ and XOY coordinate systems.

Figure 5 shows the transformation of received noise between IOQ and XOY coordinate systems, where IOQ and XOY coordinate systems denote the coordinate system for Gray mapping and rotated mapping, respectively. N_{I} and N_{Q} denote the noise on I and Q axes, respectively, which are *independent and identically distributed* (i.i.d) and both $\mathcal{N}(0, \sigma_n^2)$ distributed. Let N_{X} and N_{Y} be the noises on X and Y axes. The synthetic noise, $z = N_{\mathrm{I}} + jN_{\mathrm{Q}}$, is a *zero mean circular symmetric complex Gaussian noise* (ZMCSCGN) and $\mathcal{CN}(0, 2\sigma_n^2)$ distributed. From the transformation as shown in Fig. 5, N_{X} and N_{Y} can be calculated from N_{I} and N_{Q} as

$$\begin{aligned} N_{\mathrm{X}} &= N_{\mathrm{I}} \cos\alpha + N_{\mathrm{Q}} \sin\alpha, \\ N_{\mathrm{Y}} &= N_{\mathrm{I}} \sin\alpha + N_{\mathrm{Q}} \cos\alpha. \end{aligned} \tag{4}$$

And thus, the expected value and variance of N_{X} can be calculated as

$$\begin{aligned} \mathrm{E}(N_{\mathrm{X}}) &= 0, \\ \mathrm{Var}(N_{\mathrm{X}}) &= \mathrm{E}\left(N_{\mathrm{I}}^2 \cos^2\alpha + 2N_{\mathrm{I}}N_{\mathrm{Q}} \cos\alpha \sin\alpha + N_{\mathrm{Q}}^2 \sin^2\alpha\right) \\ &= \mathrm{E}\left(N_{\mathrm{I}}^2\right) \cos^2\alpha + \mathrm{E}\left(2N_{\mathrm{I}}N_{\mathrm{Q}}\right) \cos\alpha \sin\alpha \\ &\quad + \mathrm{E}\left(N_{\mathrm{Q}}^2\right) \sin^2\alpha \\ &= \sigma_n^2. \end{aligned} \tag{5}$$

Similarly, we can obtain the expected value and variance of N_{Y} as

$$\mathrm{E}(N_{\mathrm{Y}}) = 0 \text{ and } \mathrm{Var}(N_{\mathrm{Y}}) = \sigma_n^2. \tag{6}$$

From (4), (5) and (6), the noise mapping to the rotated coordinate system, XOY, is still Gaussian distributed with zero mean and variance σ_n^2, that is, $N_{\mathrm{X}}, N_{\mathrm{Y}} \sim \mathcal{N}(0, \sigma_n^2)$. The above derivation and conclusion also validate the ZMCSCGN characteristics of $z = N_{\mathrm{I}} + jN_{\mathrm{Q}}$.

For rotated mapping QAM in Fig. 4, the constellation and the coordinate system are both rotated with an angle α, and thus the bits for X and Y axes are mapped into real and

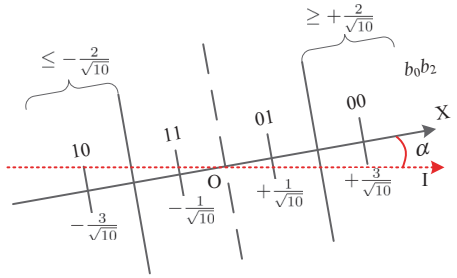

Fig. 6. The transformation of received noise between IOQ and XOY coordinate systems.

imaginary parts of the constellation point in XOY coordinate system independently as the mapping relation in IOQ coordinate system [15]. In this case, we only analyze the error characteristics for X axis. All conclusions for X axis can be directly extended to those for Y axis. Here we take the error characteristics for X axis of rotated mapping 16-QAM as an example, which can be illustrated as Fig. 6.

From Fig. 6, we can find that the decision threshold of b_0 is Y axis, that is, $X = 0$, while the decision threshold of b_2 is the line of $X = \pm 2/\sqrt{10}$. $p_n^{\mathrm{X}}, p_n^{\mathrm{Y}} \in \left\{\pm 1/\sqrt{10}, \pm 3/\sqrt{10}\right\}$ denote the transformed coordinates of the n-th transmitted symbol p_n on X and Y axes, respectively, which are just the rotated version of p_n with rotated angle α. Assuming $p_n^{\mathrm{X}} = +3/\sqrt{10}$, the probability of error decision for b_0 can be expressed as

$$P_{\mathrm{e}}\left(b_0 | p_n^{\mathrm{X}} = +3/\sqrt{10}\right) = \int_{-\infty}^{0} \frac{1}{\sqrt{2\pi}\sigma_n} \mathrm{e}^{-\frac{\left(x-3/\sqrt{10}\right)^2}{2\sigma_n^2}} \mathrm{d}x = Q\left(\frac{3}{\sqrt{10}\sigma_n}\right), \tag{7}$$

where the error function $Q(x)$ is defined as $Q(x) = \frac{1}{\sqrt{2\pi}} \int_x^{+\infty} \mathrm{e}^{-\frac{t^2}{2}} dt$.

Similarly, when other symbols are transmitted, the probability of error decision for b_0 can be calculated as

$$P_{\mathrm{e}}\left(b_0 | p_n^{\mathrm{X}} = -3/\sqrt{10}\right) = \int_{0}^{+\infty} \frac{1}{\sqrt{2\pi}\sigma_n} \mathrm{e}^{-\frac{\left(x+3/\sqrt{10}\right)^2}{2\sigma_n^2}} \mathrm{d}x = Q\left(\frac{3}{\sqrt{10}\sigma_n}\right) \tag{8}$$

and

$$P_{\mathrm{e}}\left(b_0 | p_n^{\mathrm{X}} = \pm 1/\sqrt{10}\right) = \int_{0}^{+\infty} \frac{1}{\sqrt{2\pi}\sigma_n} \mathrm{e}^{-\frac{\left(x+1/\sqrt{10}\right)^2}{2\sigma_n^2}} \mathrm{d}x = Q\left(\frac{1}{\sqrt{10}\sigma_n}\right). \tag{9}$$

When the probabilities for the transmitted symbols are equal, the total probabilities of error decision for b_0 is given by

$$P_{\mathrm{e}}(b_0) = \frac{1}{2}\left(Q\left(\frac{3}{\sqrt{10}\sigma_n}\right) + Q\left(\frac{1}{\sqrt{10}\sigma_n}\right)\right). \tag{10}$$

According to (7), (8), (9) and (10), the total probability of error decision for b_2 is given by

$$P_{\mathrm{e}}(b_2) = \frac{1}{2}Q\left(\frac{3}{\sqrt{10}\sigma_n}\right) + Q\left(\frac{1}{\sqrt{10}\sigma_n}\right) - \frac{1}{2}Q\left(\frac{5}{\sqrt{10}\sigma_n}\right). \tag{11}$$

As $Q\left(\frac{1}{\sqrt{10}\sigma_n}\right) \gg Q\left(\frac{3}{\sqrt{10}\sigma_n}\right) \gg Q\left(\frac{5}{\sqrt{10}\sigma_n}\right)$, we have $P_{\mathrm{e}}(b_0) \ll P_{\mathrm{e}}(b_2)$. Similarly, for Y axis, we have $P_{\mathrm{e}}(b_1) \ll P_{\mathrm{e}}(b_3)$.

From the previous derivation, it can be concluded that b_0 and b_1 have better error protection capabilities than b_2 and b_3 for rotated mapping 16-QAM.

4.2 Key-Bit Protection for 3D-Turbo Codes

As analyzed in [2], among the bits of 3D-Turbo codes, the systematic bits directly corresponding to the source bits and the post-encoded parity bits have important influence on the error performance. The extrinsic information of the post-encoded bits is transferred between Turbo decoder and pre-decoder. Some error propagation emerging on these extrinsic information will result in significant degradation of performance. Consequently, these two types of bits need protecting. Based on the UEP capability of rotated mapping QAM in Sec. 4.1, we develop a key-bit protection scheme described as follows.

(1) seek the bits with high error protection capability for rotated mapping QAM through the same derivation in Sec. 4.1;

(2) extract the key bits from 3D-Turbo code, such as systematic bits and the post-encoded parity bits [2];

(3) arrange the key bits extracted in Step (2) in the positions where the bits for rotated mapping QAM have high error protection capability as sought in Step (1). For example, when considering rotated mapping 16-QAM, b_0 and b_2 can be used to transmit the key bits, such as systematic bits and the post-encoded bits, while b_1 and b_3 can be done to transmit the other bits;

(4) configure this arrangement as the interleaver pattern, π, of our proposed BICM system, described in Sec. 6.

5. Soft Demodulation of QAM over Rayleigh Fading Channel

In this paper, we will construct the BICM system in Section 6 by combining 3D-Turbo code and rotated mapping QAM. Therefore, QAM demodulator needs to provide *log-likelihood ratio* (LLR) information of each bit for 3D-Turbo decoder. Thus hard demodulation of QAM no longer applies. In this section, based on MAP algorithm [5], we will

derive the soft demodulation of QAM over Rayleigh fading channel without or with a priori information from 3D-Turbo decoder.

5.1 Rayleigh Channel

In a mobile communication environment, signals are usually assumed to be propagated over Rayleigh fading channel. Over this channel, the transmitted symbol x will experience both multiplication noise and additive noise, and the received symbol y can be formulated as

$$y = \rho x + z \tag{12}$$

where ρ denotes the Rayleigh fading coefficient, and the additive noise z is $\mathcal{CN}(0, 2\sigma_n^2)$ with the variance σ_n^2 for the noise on both I and Q axes.

At receiver, if the fading coefficient ρ is perfectly estimated and the transmitted symbol x is known, the conditional *probability density function* (PDF) of a given received symbol y is expressed as [16]

$$P(y|x,\rho) = \frac{1}{2\pi\sigma_n^2} \mathrm{e}^{-\frac{\|y-\rho x\|^2}{2\sigma_n^2}}. \tag{13}$$

5.2 Classical Soft Demodulation of QAM without A Priori Information

For M-QAM ($M = 2^m$), a constellation point can be mapped by an n-bit sequence. Let $(b_0, \cdots, b_{m-1})$ be the bit sequence corresponding to any constellation point of M-QAM, x. With the received symbol y, from total probability formula, the probability of deciding bit $b_i (i = 0, \cdots, m-1)$ as $a \in \{0, 1\}$, $P(b_i = a|y)$, can be calculated by summing up the probability of each transmitting constellation point whose corresponding bit b_i is a. Therefore, $P(b_i = a|y)$ can be given by

$$\begin{aligned} P(b_i = a|y) &= \sum_{x \in \chi_a^i} P(x|y) \\ &= \sum_{x \in \chi_a^i} P(y|x) \cdot P(x) / P(y) \end{aligned} \tag{14}$$

where χ_a^i denotes the constellation point set where the i-th bit corresponding to each constellation point is a, $P(y)$ and $P(x)$ are the probabilities of received symbol y and transmitted symbol x, respectively. $P(y)$ is a constant for a given received symbol. For demodulation without a priori information, all symbols are assumed to be transmitted with equal probability. In this case, we have $P(x) = 1/2^m = 1/M$.

For soft demodulation of QAM, if received symbol is y, the LLR of the i-th bit, b_i, can be calculated as [17]

$$\begin{aligned} \mathrm{LLR}(b_i) &= \ln \frac{\sum_{x \in \chi_1^i} P(y|x) \cdot P(x)}{\sum_{x \in \chi_0^i} P(y|x) \cdot P(x)} \\ &= \ln \frac{\sum_{x \in \chi_1^i} \mathrm{e}^{-\frac{\|y-\rho x\|^2}{2\sigma_n^2}}}{\sum_{x \in \chi_0^i} \mathrm{e}^{-\frac{\|y-\rho x\|^2}{2\sigma_n^2}}}. \end{aligned} \tag{15}$$

Note that, $P(x)$ in (14) and (15) are implicitly equivalent to $P(x|b_i = a)$ due to the valid set χ_a^i.

5.3 Soft Demodulation of QAM with A Priori Information

If the a priori information about the transmitted symbol is available, the performance of soft demodulation of QAM can be significantly improved. In the subsection, we fully utilize the extrinsic information about each transmitted bit, provided by 3D-Turbo decoder, to compute the a priori information about the transmitted symbol. With the a priori information, the soft demodulation can be implemented as Fig. 7.

Let $(a_0, \cdots, a_{m-1})$ be the corresponding bit sequence of a given transmitted symbol x, where $a_i \in \{0, 1\}$ for $i = 0, \cdots, m-1$. If the i-th bit of bit sequence for x is confirmed to be a_i, the conditional probability of transmitting symbol x can be calculated as

$$P(x|b_i = a_i) = \prod_{l=0, l \neq i}^{m-1} P_{\mathrm{Turbo}}(b_l = a_l) \tag{16}$$

where $P_{\mathrm{Turbo}}(b_l = a_l)$ $(l = 0, \cdots, m-1)$ denotes the posterior probability of $b_l = a_l$ provided by 3D-Turbo decoder. For the initial demodulation, no posterior probability of $b_l = a_l$ can be applied. And thus, the probability of transmitted symbol x given $b_i = a_i$ is assumed to be $P(x|b_i = a_i) = 1/2^n$ uniformly for $i = 0, 1, \cdots, m-1$.

For clarity, we still take the soft demodulation of 16-QAM as an example to illustrated the computation of conditional probability $P_{\mathrm{Turbo}}(b_i = a_i)$. Denote $P_i^1 = P_{\mathrm{Turbo}}(b_i = 1)$ and $P_i^0 = P_{\mathrm{Turbo}}(b_i = 0)$ as the probabilities of the i-th bit b_i being 1 and 0, respectively. $P_{\mathrm{Turbo}}(b_i = 1)$ and $P_{\mathrm{Turbo}}(b_i = 0)$ are derived from the extrinsic information about b_i output by 3D-Turbo decoder [11]. When calculating the probability of $P(b_0 = 1|y)$, the probabilities of all transmitted symbols whose first bit b_0 is 1, $P(x|b_0 = 1)$, are required. Further assuming the bit sequence of transmitted symbol $\tilde{x}$ is $(b_0 b_1 b_2 b_3) = (1010)$, the probability of transmitting $\tilde{x}$ can be given as $P(\tilde{x}|b_0 = 1) = P_1^0 \times P_2^1 \times P_3^0$ from (16).

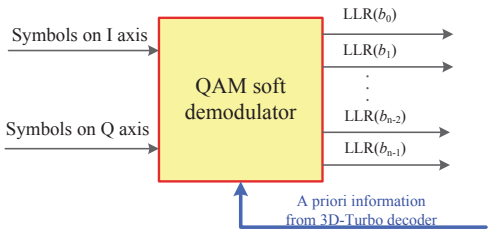

Fig. 7. Soft demodulation with a priori information from 3D-Turbo decoder.

Combining the a priori information about the transmitted symbol in (16), we can re-formulate the LLR of the i-th bit as

$$\begin{aligned}\mathrm{LLR}\left(b_i\right) &= \ln \frac{\sum\limits_{x\in\chi_1^i} P\left(y|x\right)\cdot P\left(x|b_i=1\right)}{\sum\limits_{x\in\chi_0^i} P\left(y|x\right)\cdot P\left(x|b_i=0\right)} \\ &= \ln \frac{\sum\limits_{x\in\chi_1^i}\left(P\left(y|x\right)\cdot\prod\limits_{l=0,l\neq i}^{n-1} P_{\mathrm{Turbo}}\left(b_l=a_l\right)\right)}{\sum\limits_{x\in\chi_0^i}\left(P\left(y|x\right)\cdot\prod\limits_{l=0,l\neq i}^{n-1} P_{\mathrm{Turbo}}\left(b_l=a_l\right)\right)}.\end{aligned} \tag{17}$$

6. A Novel BICM System Combining 3D-Turbo Code and Rotated Mapping QAM

As analyzed in [2], [3], [10] and [11], 3D-Turbo code achieves good BER performance over AWGN channel. In this section, we will propose a novel BICM system by combining 3D-Turbo code and rotated mapping QAM. In this system, key-bit protection scheme and 2D iterative soft demodulating-decoding algorithm are developed to improve the BER performance of 3D-Turbo code over Rayleigh fading channel.

6.1 Procedure for Transmitter

At transmitter, we adopted rotated mapping QAM with cyclic shift and key-bit error protection scheme. The transmitter including 3D-Turbo encoder, bit interleaver and modulator of rotated mapping is shown as Fig. 8.

In Fig. 8, the modules connected by broken line represent the operations of classical Gray mapping QAM, while those connected by full line represent the operations of rotated mapping QAM. In our proposed BICM transmitter, two techniques are implemented. (1) To fulfill independent fading for the symbols on I and Q axes, the symbols on Q axis are cyclicly shifted with K symbols as described in Sec. 3.2. (2) To realize key-bit protection, a new bit interleaver is devised as Π in Sec. 4. With bit interleaver, Π, the key bits, such as systematic bits and post-encoded bits, are loaded by the bits with high error protection capability in rotated mapping

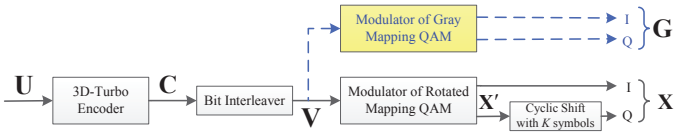

Fig. 8. BICM transmitter with 3D-Turbo encoder and rotated mapping.

QAM, and the other bits output by 3D-Turbo encoder are mapped to the rest bits in rotated mapping QAM.

To sum up, the procedure of the transmitter in the BICM system can be described as follows:

(1) the information bits, **U**, are firstly encoded by 3D-Turbo encoder to get 3D-Turbo code **C**;

(2) the code **C** is then interleaved with Π to form transmitted sequence **V**;

(3) the transmitted sequence **V** is mapped into symbols **X′** by modulator of rotated mapping QAM. The symbols of **X′** on I axis and the K cyclicly-shifted symbols of **X′** on Q axis are combined to form transmitted symbols $\mathbf{X} = (x_0, x_1, \cdots, x_{N-1})$, where N denotes the number of transmitted symbols;

(4) the transmitted symbols, **X**, are finally sent into channel for transmission.

6.2 Procedure for Receiver

At receiver, we propose a 2D iterative soft demodulating-decoding algorithm to achieve BER performance improvement, which can be illustrated as Fig. 9. The modules for classical Gray mapping QAM connected with broken line are also included in Fig. 9.

From Fig. 9, when 2D iterative soft demodulating-decoding algorithm is implemented, the demodulator of rotated mapping QAM utilizes the extrinsic information provided by 3D-Turbo decoder to compute the a priori probability of each transmit symbol and does soft demodulation; and the 3D-Turbo decoder takes the LLR information for each bit output by demodulator as soft input to fulfill SISO decoding procedure. The iterative information exchange benefits the performance improvement. In summary, 2D iterative detection in Fig. 9 represents the iteration inside 3D-Turbo decoder and iteration between soft QAM demodulator and 3D Turbo decoder.

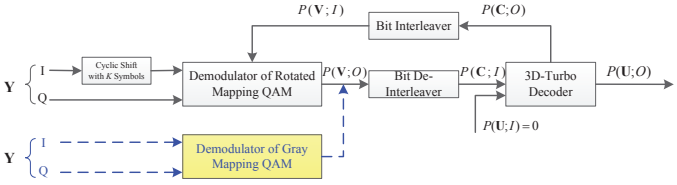

Fig. 9. BICM receiver with 3D-Turbo encoder and rotated mapping.

Let $\mathbf{Y} = (y_0, y_1, \cdots, y_{N-1})$ be the received symbols at receiver corresponding to $\mathbf{X}$.

Due to cyclic shift with K symbols for rotated mapping QAM, the symbols on I and Q axes for the same constellation point experience different fading of the channel. Therefore, the soft demodulation in (17) must be modified. Considering the transmitted complex symbols in (3), the received complex symbols at time $n(0 \le n \le N-1)$ can be denoted as

$$y_n = \rho_n x_n + z_n = \rho_n \left(x_n^{\mathrm{I}} + j x_n^{\mathrm{Q}}\right) + z_n \tag{18}$$

where $x_n^{\mathrm{I}} = \mathrm{Re}(x_n)$, $x_n^{\mathrm{Q}} = \mathrm{Im}(x_n)$ and z_n represents a ZMCSCGN with PDF $\mathcal{CN}(0, 2\sigma_n^2)$.

From (18), we have

$$\tilde{y}_n = \frac{y_n}{\rho_n} = x_n^{\mathrm{I}} + j x_n^{\mathrm{Q}} + \frac{z_n}{\rho_n}. \tag{19}$$

In (19), due to the circular characteristics of z_n, $\tilde{z}_n = \frac{z_n}{\rho_n}$ is still a ZMCSCGN and thus $\tilde{z}_n \sim \mathcal{CN}\left(0, \frac{2\sigma_n^2}{\|\rho_n\|^2}\right)$ where $\|\cdot\|$ denotes the amplitude of a complex. Further let $\tilde{y}_n^{\mathrm{I}} = \mathrm{Re}(\tilde{y}_n)$, $\tilde{y}_n^{\mathrm{Q}} = \mathrm{Im}(\tilde{y}_n)$, $\tilde{z}_n^{\mathrm{I}} = \mathrm{Re}(\tilde{z}_n)$ and $\tilde{z}_n^{\mathrm{Q}} = \mathrm{Im}(\tilde{z}_n)$. For ZMCSCGN $\tilde{z}_n \sim \mathcal{CN}\left(0, \frac{2\sigma_n^2}{\|\rho_n\|^2}\right)$, we have $\tilde{z}_n^{\mathrm{I}}, \tilde{z}_n^{\mathrm{Q}} \sim \mathcal{N}\left(0, \frac{\sigma_n^2}{\|\rho_n\|^2}\right)$. Divide (19) into real and imaginary parts as

$$\begin{aligned} \tilde{y}_n^{\mathrm{I}} &= x_n^{\mathrm{I}} + \tilde{z}_n^{\mathrm{I}}, \\ \tilde{y}_n^{\mathrm{Q}} &= x_n^{\mathrm{Q}} + \tilde{z}_n^{\mathrm{Q}}. \end{aligned} \tag{20}$$

In this paper, the fading coefficient, ρ_n, is assumed to be perfectly estimated. In this case, from (19) and based on the statistics of $\tilde{z}_n^{\mathrm{I}}$ and $\tilde{z}_n^{\mathrm{Q}}$, the conditional PDFs can be expressed as

$$P(\tilde{y}_n^{\mathrm{I}} | x_n^{\mathrm{I}}) = \frac{\|\rho_n\|}{\sqrt{2\pi}\sigma_n} \mathrm{e}^{-\frac{\left(\tilde{y}_n^{\mathrm{I}} - x_n^{\mathrm{I}}\right)^2 \|\rho_n\|^2}{2\sigma_n^2}} \tag{21}$$

and

$$P(\tilde{y}_n^{\mathrm{Q}} | x_n^{\mathrm{Q}}) = \frac{\|\rho_n\|}{\sqrt{2\pi}\sigma_n} \mathrm{e}^{-\frac{\left(\tilde{y}_n^{\mathrm{Q}} - x_n^{\mathrm{Q}}\right)^2 \|\rho_n\|^2}{2\sigma_n^2}}, \tag{22}$$

respectively.

From (3) in Section 3.2, we can find the inverse relationship between $\mathbf{P}$ and $\mathbf{X}$ as

$$p_n = x_n^{\mathrm{I}} + j x_{n'}^{\mathrm{Q}} \tag{23}$$

where $x_n^{\mathrm{I}} = \mathrm{Re}(x_n)$, $x_{n'}^{\mathrm{Q}} = \mathrm{Im}(x_{n'})$ and

$$n' = \begin{cases} n + K, & \text{if } 0 \le n \le N-1-K \\ n + K - N, & \text{if } N - K \le n \le N-1 \end{cases}. \tag{24}$$

Here, p_n denotes the symbol of rotated mapping QAM without cyclic shift.

Therefore, the conditional PDF of p_n given the received symbols $\mathbf{Y}$ can be calculated as

$$\begin{aligned} P(p_n|\mathbf{Y}) &= P(x_n^{\mathrm{I}} + j x_{n'}^{\mathrm{Q}} | \mathbf{Y}) \\ &= P(x_n^{\mathrm{I}}|\mathbf{Y}) P(x_{n'}^{\mathrm{Q}}|\mathbf{Y}) \\ &= P(x_n^{\mathrm{I}}|\tilde{y}_n^{\mathrm{I}}) P(x_{n'}^{\mathrm{Q}}|\tilde{y}_{n'}^{\mathrm{Q}}) \\ &= \frac{P(\tilde{y}_n^{\mathrm{I}}|x_n^{\mathrm{I}}) P(x_n^{\mathrm{I}})}{P(\tilde{y}_n^{\mathrm{I}})} \cdot \frac{P(\tilde{y}_{n'}^{\mathrm{Q}}|x_{n'}^{\mathrm{Q}}) P(x_{n'}^{\mathrm{Q}})}{P(\tilde{y}_{n'}^{\mathrm{Q}})} \\ &= \frac{P(\tilde{y}_n^{\mathrm{I}}|x_n^{\mathrm{I}}) P(\tilde{y}_{n'}^{\mathrm{Q}}|x_{n'}^{\mathrm{Q}})}{P(\tilde{y}_n^{\mathrm{I}}) P(\tilde{y}_{n'}^{\mathrm{Q}})} \cdot P(x_n^{\mathrm{I}}) P(x_{n'}^{\mathrm{Q}}) \\ &= \frac{P(\tilde{y}_n^{\mathrm{I}}|x_n^{\mathrm{I}}) P(\tilde{y}_{n'}^{\mathrm{Q}}|x_{n'}^{\mathrm{Q}})}{P(\tilde{y}_n^{\mathrm{I}}) P(\tilde{y}_{n'}^{\mathrm{Q}})} \cdot P(p_n). \end{aligned} \tag{25}$$

In (25), $P(\tilde{y}_n^{\mathrm{I}})$ and $P(\tilde{y}_{n'}^{\mathrm{Q}})$ are included. In the following part, we will derive the PDF of $\tilde{y}_n^{\mathrm{I}}$ as

$$\begin{aligned} P(\tilde{y}_n^{\mathrm{I}}) &= P(y_n) = P(y_n, \chi) \\ &= \sum_{w \in \chi} P(y_n, w) = \sum_{w \in \chi} P(y_n|w) P(w) \\ &= \sum_{w \in \chi} \left(\frac{1}{2\pi\sigma_n^2} \mathrm{e}^{-\frac{\|y_n - \rho_n w\|^2}{2\sigma_n^2}} \cdot P(w) \right) \end{aligned} \tag{26}$$

where the first equation is based on the reality that $\tilde{y}_n^{\mathrm{I}}$ includes all the information of y_n when ρ_n is perfectly estimated and χ denotes the whole constellation. Actually, in (26), the summation is implemented for all the constellation points.

As the derivation in (26), we can obtain the PDF of $\tilde{y}_n^{\mathrm{Q}}$ as

$$P(\tilde{y}_n^{\mathrm{Q}}) = \sum_{w \in \chi} \left(\frac{1}{2\pi\sigma_n^2} \mathrm{e}^{-\frac{\|y_n - \rho_n w\|^2}{2\sigma_n^2}} \cdot P(w) \right). \tag{27}$$

From (26) and (27), we can conclude that all $P(\tilde{y}_n^{\mathrm{I}})$ and $P(\tilde{y}_n^{\mathrm{Q}})$ are identical for $n = 0, 1, \cdots, N-1$.

As (17), with (21), (22), (25) and the conclusion of identical PDFs of $\tilde{y}_n^{\mathrm{I}}$ and $\tilde{y}_n^{\mathrm{Q}}$, we can calculate the LLR as (28) in the 8-th page. In (28), p_n denotes the symbol without cyclic shift, $p_n^{\mathrm{I}} = \mathrm{Re}(p_n)$, $p_n^{\mathrm{Q}} = \mathrm{Im}(p_n)$, and the a priori probability of p_n, $P(p_n | b_i = a)(a \in \{0, 1\})$, can be computed as (16).

In the end, the procedure of the receiver in the proposed BICM system can be concluded as follows:

(1) initialize the a priori information of the demodulator of rotated mapping QAM, $P_{\mathrm{Turbo}}(b_l = a_l) = 1/2$;

(2) cyclicly shift the symbols on I axis by K symbols to align the symbols on Q axis. The cyclicly-shifted symbols on I axis and the symbols on Q axis are transferred into the demodulator of rotated mapping QAM to compute the LLR information of the transmitted sequence $\mathbf{V}$, $P(\mathbf{V}; O)$, with (28) in the 8-th page;

(3) deinterleave $P(\mathbf{V}; O)$ according to bit interleaver Π and get the soft input of 3D-Turbo decoder, $P(\mathbf{C}; I)$;

$$\mathrm{LLR}\left(b_i\right)=\ln\frac{\sum\limits_{p_n\in\chi_1^i}\frac{\|\rho_n\|\|\rho_{n'}\|}{2\pi\sigma_n^2}\mathrm{e}^{-\frac{\left(\tilde{y}_n^{\mathrm{I}}-p_n^{\mathrm{I}}\right)^2\|\rho_n\|^2+\left(\tilde{y}_{n'}^{\mathrm{Q}}-p_n^{\mathrm{Q}}\right)^2\|\rho_{n'}\|^2}{2\sigma_n^2}}\cdot P\left(p_n|b_i=1\right)}{\sum\limits_{p_n\in\chi_0^i}\frac{\|\rho_n\|\|\rho_{n'}\|}{2\pi\sigma_n^2}\mathrm{e}^{-\frac{\left(\tilde{y}_n^{\mathrm{I}}-p_n^{\mathrm{I}}\right)^2\|\rho_n\|^2+\left(\tilde{y}_{n'}^{\mathrm{Q}}-p_n^{\mathrm{Q}}\right)^2\|\rho_{n'}\|^2}{2\sigma_n^2}}\cdot P\left(p_n|b_i=0\right)}. \tag{28}$$

(4) initialize the a priori information of the 3D-Turbo decoder, $P(\mathbf{U};I)=0$; 3D-Turbo decodes $P(\mathbf{C};I)$ to get the LLR information of the information bit $\mathbf{U}$, $P(\mathbf{U};O)$, and the extrinsic information of the encoded codes $\mathbf{C}$, $P\left(\mathbf{C};O\right)$, according to the algorithms in [11];

(5) as long as the iteration counter reaches the configured maximum iterations, stop the 2D iterative soft demodulating-decoding algorithm and output the estimated information bits by hard decision of $P(\mathbf{U};O)$; otherwise, compute $P_{\text{Turbo}}\left(b_l=a_l\right)$ according to (16) with the interleaved $P\left(\mathbf{C};O\right)$, and feed $P(\mathbf{V};I)$ composed by $P_{\text{Turbo}}\left(b_l=a_l\right)$ to the demodulator as its a priori information of each transmitted symbol, and return to Step (2).

Note that, to reduce the operations and save computation time, the iterations of demodulating can be set to be less than those of 3D-Turbo decoding. In the initial several iterations, the 2D iterative soft demodulating-decoding algorithm keeps working. However, in the following iterations, maintain the previous output of demodulator, $P(\mathbf{V};O)$, as the soft input of 3D-Turbo decoder. In the latter case, the demodulator is not included in the iterative procedure. This configuration can be proved to have little influence on the performance in Sec. 7.

7. Simulation Results and Analysis

In this section, some simulation results are presented to validate the improvement of BER performance. The simulation parameters are listed in Tab. 1. Due to perfect estimation of fading channel, the number of cyclicly-shifted symbols is set to be $K=1$, without loss of generality.

Figure 10 compares the soft demodulation performance of Gray mapping and rotated mapping QAM over Rayleigh fading channel without considering channel coding. The rotated mapping QAM can increase the signal diversity, and the received symbols on both I and Q axes can provide information for demodulator while only the received symbol on I or Q axis can offer information in Gray mapping QAM. Therefore, compared with classical Gray mapping QAM, rotated mapping QAM have better BER performance and can obtain about 7 dB gain at BER $=10^{-4}$ over Rayleigh fading channel.

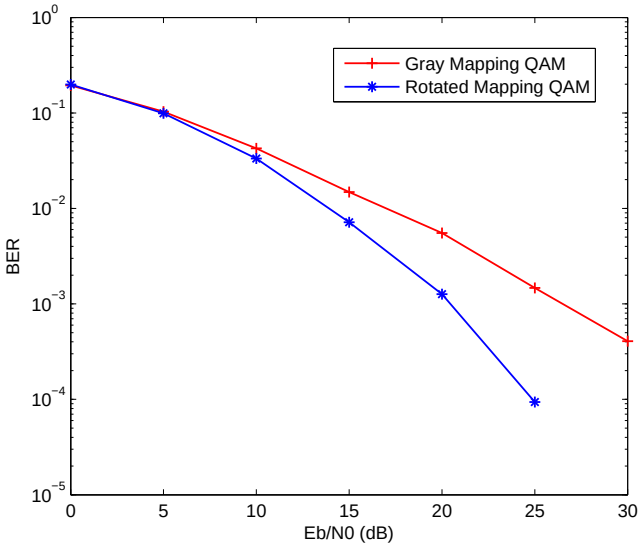

Fig. 10. Soft demodulation performance of Gray mapping and rotated mapping QAM over Rayleigh fading channel without considering channel coding.

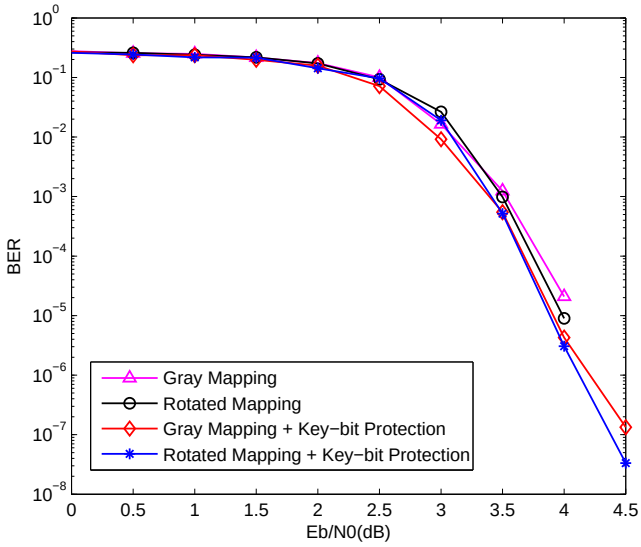

Fig. 11. Performance of different coded-modulation schemes over AWGN channel.

Figure 11 shows performance comparison between Gray mapping QAM and Rotation mapping QAM and validates the improvement of key-bit protection over AWGN channel. In this comparison, no iterative demodulating-decoding algorithm is considered.

Type	Parameter	Configuration
QAM	Order	Rotated mapping 16-QAM
	Rotation angle	16.8°
	Symbols of cyclic shift	$K = 1$
3D-Turbo code	Length of information bits	$L = 570$
	Rate	$R = \frac{1}{3}$
	Permeability rate	$\lambda = \frac{1}{4}$
	Polynomials of Turbo encoder	$(15, 13)_8$
	Polynomials of post-encoder	$(5, 4)_8$
	Interleaver of Turbo encoder π	interleaver in [18]
	Interleaver of post-encoder π'	interleaver in [19] ($L_0 = 23, i_0 = 11$)
	Decoding algorithm	Max-LogMAP
	Number of iterations	10
Channel	Channel estimation	Perfect

Tab. 1. Parameter configuration for simulations.

From Fig. 11, over AWGN channel, rotated mapping QAM shows a little worse BER performance than Gray mapping QAM at low-medium SNRs (< 3.3 dB) while the former outperforms the latter at high SNRs. Compared with Gray mapping QAM, rotated mapping QAM achieves 0.2 dB gain at BER = 10^{-5}. When key-bit protection scheme is considered, these two mapping QAMs have the same trend in terms of BER performance and rotated mapping QAM achieves 0.3 dB gain at BER = 10^{-5} compared with Gray mapping QAM. In total, the key-bit protection scheme slightly improves the performance of BICM system over AWGN channel. At high SNRs, rotated mapping QAM makes use of high diversity from both I and Q axes to achieve better performance while Gray mapping QAM only uses the soft information from I or Q axis. However, at low-medium SNRs, rotated mapping QAM suffers from noise pollution feasibly and has a little performance degradation due to smaller distance between neighbor coordinates on I or Q axis.

To highlight the superiority of our proposed scheme, we construct three BICM systems by combining 3D-Turbo code with Gray-mapped QAM, rotated mapping QAM without iterative processing, and rotated mapping QAM with 2D iterative soft demodulating-decoding algorithm, respectively. These three systems all adopt the key-bit protection scheme. The BER performance of the three systems is compared in Fig. 12.

From Fig. 12, the BICM system with rotated mapping QAM has almost the same performance as that with Gray mapping QAM at low-medium SNRs (< 5.5 dB) while the former obtains a few gain over the latter at high SNRs. For BICM system with rotated mapping QAM, the improvement at high SNRs benefits from the utilization of information from both I and Q axes. Compared with these two system, the BICM system with rotated mapping QAM and 2D iterative soft demodulating-decoding algorithm achieves a larger gain of 0.8-1.0 dB at BER = 10^{-6}. In our proposed BICM system, the a priori information from 3D-Turbo decoder can increase the performance of demodulator. The improved

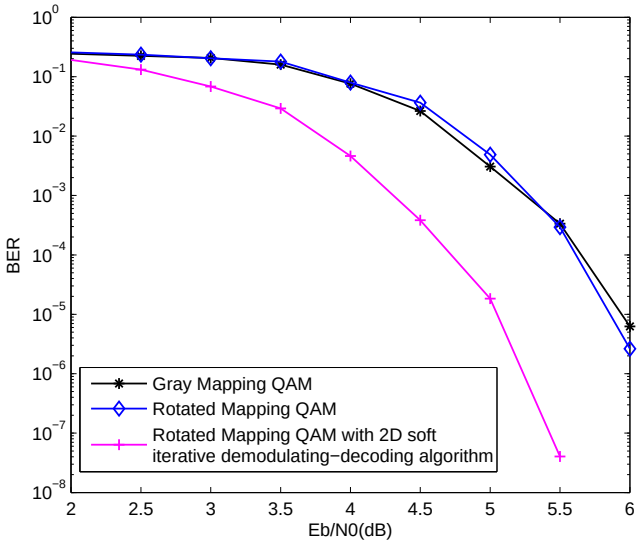

Fig. 12. Performance of different coded-modulation schemes over Rayleigh fading channel.

LLRs from demodulator, in return, improve the BER performance of 3D-Turbo decoder. In general, the proposed scheme can improve the BER performance.

However, the improvement of our proposed scheme is at sacrifice of complexity and delay. Due to the adoption of 3D Turbo codes and iterative processing of demodulator and decoder, the complexity of our scheme is surely increased. In [11], we have compared the complexity between 3D Turbo codes and classical Turbo codes. For typical parameters, 3D Turbo decoder requires 7.2 % more additions and 17.3 % more comparison-selections than classical Turbo decoder does. From that comparison, the complexity from 3D Turbo codes is not high. The iterative processing will introduce little complexity for iteration control and some delay rather than prominent complexity. With the increasing processing capability of modern processor, the complexity may be solvable and out of question. Furthermore, when some systems pursuit the BER improvement, the limited complexity increase is worthwhile. Note that, some pipeline

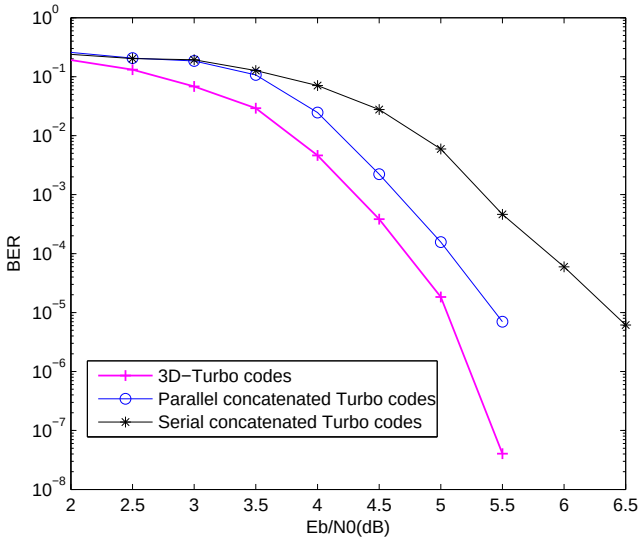

Fig. 13. Comparison of BER performance for different Turbo codes.

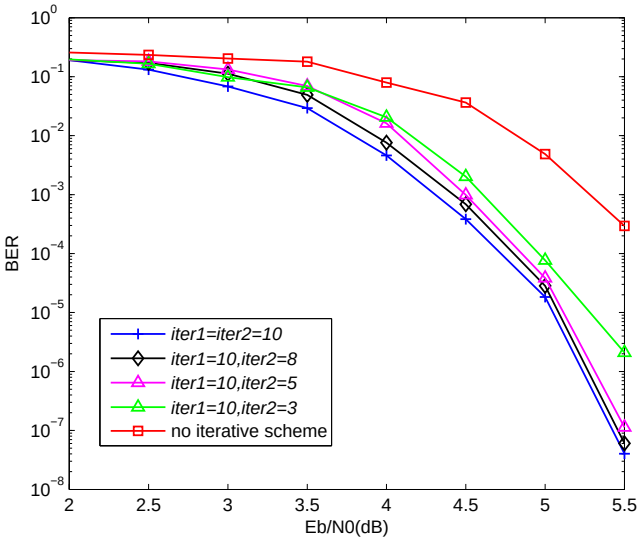

Fig. 14. The influence of different iterations on BER performance for 2D iterative demodulating-decoding algorithm.

or parallelized processing techniques can efficiently decrease the delay.

In Fig. 13, we compare the BER performance for 3D-Turbo codes, parallel or serial concatenated Turbo codes with considering key-bit protection and 2D iterative processing. For parallel concatenated Turbo codes, the information bits are the key bits, while the information bits for outer encoder are the key bits for serial concatenated Turbo codes. From Fig. 13, we can find prominent improvement of our proposed scheme over the other two codes. Parallel concatenated Turbo codes show worse performance due to their high error floor; moreover, serial concatenated Turbo codes show even the worst performance because half of the soft information fed back to soft QAM demodulator are contributed only by inner decoder rather than both inner and outer decoder.

For the 2D iterative soft demodulating-decoding algorithm in BICM system, we can set different iterations for 3D-Turbo decoder and joint demodulating-decoding processing. Denote $iter1$ and $iter2$ as the iterations for 3D-Turbo decoder and joint demodulating-decoding processing, respectively. Figure 14 shows the influence of different iterations on BER performance for 2D iterative demodulating-decoding algorithm.

From Fig. 14, when $iter2 < iter1$, iterations have a significant impact on system performance at low SNRs. However, with the increasing of SNR, the exchanging information between demodulator and decoder approaches constant quickly and therefore proper reduction of $iter2$ will not influence the BER performance. For the non-iterative scheme, no extrinsic information from 3D-Turbo decoder feeds into demodulator. Compared with the non-iterative scheme, our proposed 2D iterative scheme achieves a large gain at all SNRs. In the implementation of practical system, we can properly reduce $iter2$ to lower the complexity of BICM system while guaranteeing the performance.

8. Conclusion and Future Work

To improve the BER performance over Rayleigh fading channel, a novel BICM system by combining 3D-Turbo code and rotated mapping QAM has been proposed. A key-bit protection scheme and a 2D iterative soft demodulating-decoding algorithm have been developed for the proposed system. The procedures for transmitter and receiver are devised in detail. Simulation results have shown our proposed BICM system can achieve BER performance improvement, which validate the feasibility of this proposed system. Considering the practical mobile communications, this system will be of great value to engineering fields for high capacity data transmission over fading channels.

In this paper, we have presented some simulation results and theoretical analysis. For straightforward scientific contribution, implementation on a hardware platform and evaluation of the proposed scheme on a practical channel are still required. These works are full of challenges, such as quantization of metrics, simplification of complicated operations, throughput improvement with pipeline techniques, and trade-off of complexity and performance. We will consider all the aspects as our future work and try to evaluate the practical performance in an ideal or real radio channel.

Acknowledgments

This work has been supported in part by the National Natural Science Foundation of China (No. 61501376 and 61301093), the Natural Science Basic Research Plan in Shaanxi Province of China (No. 2014JM2-6094), the Fundamental Research Funds for the Central Universities (No. 310832151095 and 3102016ZY020) and the Graduate Starting Seed Fund of Northwestern Polytechnical University (No. Z2016108).

References

[1] BERROU, C., GLAVIEUX, A. Near optimum error correcting coding and decoding: turbo-codes. *IEEE Transactions on Communications*, 2007, vol. 44, no. 10, p. 1261–1271. DOI: 10.1109/26.539767

[2] ISMAIL, D. K. B., DOUILLARD, C., KEROUEDAN, S. A survey of three-dimensional turbo codes and recent performance enhancements. *EURASIP Journal on Wireless Communications and Networking*, 2013, vol. 2013, p. 1–13. DOI: 10.1186/1687-1499-2013-115

[3] ISMAIL, D. K. B., DOUILLARD, C., KEROUEDAN, S. Reducing the convergence loss of 3-dimensional turbo codes. In *Proceedings of the 6th International Symposium on Turbo Codes and Iterative Information Processing (ISTC)*. Brest (France), 2010, p. 146–150. DOI: 10.1109/ISTC.2010.5613823

[4] NOUR, C. A., DOUILLARD, C. Rotated QAM constellations to improve BICM performance for DVB-T2. In *Proceedings of the 10th IEEE International Symposium on Spread Spectrum Techniques and Applications (ISSSTA)*. Bologna (Italy), 2008, p. 354–359. DOI: 10.1109/ISSSTA.2008.71

[5] LI, M., NOUR, C., JEGO, C., et al. Design of rotated QAM mapper/demapper for the DVB-T2 standard. In *Proceedings of the IEEE Workshop on Signal Processing Systems (SIPS)*. Tampere (Finland), 2009, p. 18–23. DOI: 10.1109/SIPS.2009.5336265

[6] TRAN, N., NGUYEN, H., LE-NGOC, T. Performance of BICM-ID with signal space diversity. *IEEE Transactions on Wireless Communications*, 2007, vol. 6, no. 5, p. 1732–1742. DOI: 10.1109/TWC.2007.360375

[7] LI, M., BPURDOUX, A., DEJONGHE, A., et al. A geometrical approach for highly efficient soft demodulation of rotated constellations. In *Proceedings of the IEEE Workshop on Signal Processing Systems (SIPS)*. Quebec (Canada), 2012, p. 179–184. DOI: 10.1109/SIPS.2012.63

[8] KEKRT, D., LUKES, T., KLIMA, M., et al. 2D iterative map detection: principles and applications in image restoration. *Radioengineering*, 2014, vol. 23, no. 2, p. 618–631. ISSN: 1805-9600

[9] ANASTASOPOULOS, A., CHUGG, K. M. Adaptive soft-input soft-output algorithms for iterative detection with parametric uncertainty. *IEEE Transactions on Communications*, 2000, vol. 48, no. 10, p. 1638–1649. DOI: 10.1109/26.871389

[10] ISMAIL, D. K. B. *Towards Ideal Codes: Looking for New Turbo Code Schemes*. (Ph.D. thesis), Telecomm. Bretagne, 2011.

[11] YAO, R., GAO, F., ZHANG, K., et al. Theoretical analysis and performance study of 3-dimension turbo codes. *Journal of Harbin Institute of Technology*, 2014, vol. 46, no. 11, p. 95–100. DOI: 0367-6234(2014)11-0095-06

[12] ETSI EN 302 755, V1.3.1 (2012-04). *Digital Video Broadcasting (DVB): Frame Structure Channel Coding and Modulation for a Second Generation Digital Terrestrial Television Broadcasting System (DVB-T2)*. Standard, European Telecommunications Standards Institute (ETSI), Sophia Antipolis Cedex, France, 2012.

[13] BOUTROS, J., VITERBO, E. Signal space diversity: a power- and bandwidth-efficient diversity technique for the rayleigh fading channel. *IEEE Transactions on Information Theory*, 1998, vol. 44, no. 4, p. 1453–1467. DOI: 10.1109/18.681321

[14] LI, P., CHANG, Y., FENG, N., et al. A novel hierarchical QAM-based unequal error protection scheme for H.264/AVC video over frequency-selective fading channels. *IEEE Transactions on Consumer Electronics*, 2010, vol. 56, no. 4, p. 2741–2746. DOI: 10.1109/TCE.2010.5681164

[15] SKLAR, B. *Digital Communications: Fundamentals and Applications*. New York (USA): Pearson Education Limited, 2013. ISBN: 1292026065

[16] NOUR, C. A., DOUILLARD, C. On lowering the error floor of high order turbo BICM schemes over fading channels. In *Proceedings of the IEEE Global Telecommunications Conference (GlobeCom)*. San Francisco (USA), 2006, p. 1–5. DOI: 10.1109/GLOCOM.2006.96

[17] SUN, Q., QI, W. Soft-demodulation algorithm for 64QAM and it's application in HSPA+. In *Proceedings of the 11th IEEE International Conference on Signal Processing (ICSP)*. Beijing (China), 2012, p. 2309–2312. DOI: 10.1109/ICoSP.2012.6492042

[18] 3GPP2, C.S0002-F. *Physical Layer Standard for CDMA2000 Spread Spectrum Systems*. Standard, Third Generation Partnership Project 2 (3GPP2), Seattle, 2012.

[19] BERROU, C., GRALL, I. A., MOUHAMEDOU, Y. O. C. Adding a rate-1 third dimension to turbo codes. In *Proceedings of the IEEE Information Theory Workshop (ITW)*. Lake Tahoe (USA), 2007, p. 156–161. DOI: 10.1109/ITW.2007.4313066

About the Authors ...

Rugui YAO (corresponding author) was born in Anhui, China, in 1980. He received the BS, MS and Ph.D degrees all in the School of Electronics and Information from Northwestern Polytechnical University (NPU), Xi'an, China, in 2002, 2005 and 2007, respectively. He worked as a post-doctoral fellow at NPU from 2007 to 2009. After that, he joined this school and became an associate professor in 2010. In the year of 2013, he joined ITP Lab of Georgia Tech as a visiting scholar. He has worked in the area of cognitive radio networks, channel coding, OFDM transmission and spread spectrum systems.

Yongjia ZHU was born in Henan, China, in 1992. He received his bachelor degree in the School of Electronics and Information from Northwestern Polytechnical University (NPU), Xi'an, China, in 2014 and currently he is pursuing his MS degree at NPU. His research interests include wireless communications and channel coding.

Juan XU was born in Shaanxi, China, in 1980. She received the BS, MS and Ph.D degrees all in the School of Computer from Northwestern Polytechnical University (NPU), China, in 2002, 2005 and 2011, respectively. From 2011, she joined the School of Electronic and Control Engineering at Chang'an University, Xi'an, China. Her research interests include channel coding, OFDM transmission and spread spectrum systems.